Chapter 10
Block-Type Nb_3Sn Dipole R&D at Texas A&M University

Peter McIntyre and Akhdiyor Sattarov

Abstract A succession of Nb_3Sn block-type dipoles has been developed at the Texas Agricultural and Mechanical (A&M) University and tested, in a progression of stages aimed toward 16 T operation field. This chapter describes the details of magnet design, fabrication procedures, and test results.

10.1 Introduction

The Accelerator Research Laboratory (ARL) at the Texas Agricultural and Mechanical (A&M) University has spent the past 16 years developing block-type dipole technology, with fields towards the 16 T range, as a cost-effective basis for the superconducting storage rings of a future hadron collider. The motivation for the work has been to develop coils for a dipole magnet that are easy to manufacture, and to address several aspects of dipole technology that become challenging for thick coils. At the beginning of development, stress management within the windings and correction for persistent current (Kashikhin and Zlobin 2001) due to the large filaments in high-performing Nb_3Sn strands had been seen by the accelerator magnet community as the main challenges. To address these challenges the rectangular winding geometry of a block-type geometry was selected. A cross-section and 3D sketch of the dipole coils of a block-type magnet are shown in Fig. 10.1.

The major challenge in this design option is the so-called flared-end geometry to allow for a continuous aperture and to enable the beam tube to pass through the magnet. The transition from the rectangular geometry of the body winding to the flared end is susceptible to de-registration within cables, and poses a complex challenge for stress management. So far, in this program three model dipoles (TAMU1 to TAMU3) were built using Rutherford cable, wound in flat double-pancake windings without flared ends (Diacaenko et al. 1997) to gain experience with Nb_3Sn dipole magnets. Two new model dipoles currently being developed (TAMU4 and TAMU5) utilize a novel cable-in-conduit (CIC) superconductor,

P. McIntyre (✉) · A. Sattarov
Department of Physics and Astronomy, Texas A&M University, College Station, TX, USA
e-mail: mcintyre@physics.tamu.edu; a-sattarov@physics.tamu.edu

D. Schoerling, A. V. Zlobin (eds.), *Nb_3Sn Accelerator Magnets*, Particle Acceleration and Detection, https://doi.org/10.1007/978-3-030-16118-7_10

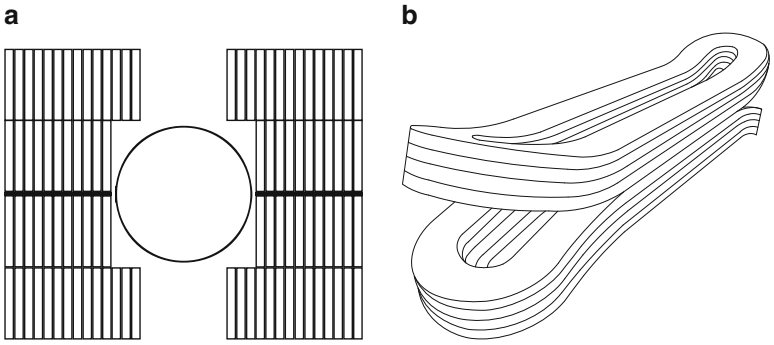

Fig. 10.1 (**a**) Coil cross-section; and (**b**) a 3D sketch of a block-type dipole magnet

Table 10.1 Summary of model dipoles built at ARL

Dipole model	Timeline	Superconductor	Field/current (T/kA)	
			Design	Achieved
TAMU1	1999–2001	Nb-Ti	6.6 T/8.1 kA	6.5 T/8.0 kA
Battle et al. (2001)				
TAMU2	2002–2006	Nb_3Sn (ITER)[a]	6.9 T/9.4 kA	6.6 T/8.9 kA
Noyes et al. (2006) and McInturff et al. (2007)				
TAMU3	2007–2013	Nb_3Sn (RRP)[b]	13 T/13.6 kA	6.6 T/7.6 kA
Blackburn et al. (2008a), Holik et al. (2011, 2014) and Elliott et al. (2016)				
TAMU4	2014–2017	Nb-Ti	4 T/15 kA	NA
Assadi et al. (2015)				
TAMU5	2016–	Nb_3Sn/Bi2212	17 T/25 kA	NA
Assadi et al. (2017)				

[a]International Thermonuclear Experimental Reactor
[b]Restacked rod process

wound in a barrel wind with flared ends. A summary of the main parameters of TAMU1 to TAMU5 is presented in Table 10.1. Due to the early stage of this work, TAMU4 and TAMU5 are not discussed in this chapter.

10.2 R&D Program and Approach

The block-type dipoles were designed, built, and tested following a strategy that focused upon one challenge or open question at a time. The main questions formulated at the beginning of the project are listed below.

1. How to manage the accumulation of Lorentz stress so that it does not produce strain in the windings beyond the limit for degradation of critical current density J_c?
2. How to suppress persistent-current multipoles due to magnetization in the superconducting filaments, which are much larger in Nb_3Sn than in Nb-Ti strands?
3. How to provide heat transfer in the inner regions of a thick winding to provide cooling and stability against micro-quenches?
4. How to support Lorentz stress in the flared ends?
5. How to form the flared ends of the winding without damaging the internal registration of the cable?
6. How to make a hybrid winding incorporating Nb-Ti windings that are not heat-treated with wind-and-react (W&R) windings of Nb_3Sn and Bi-2212?

10.2.1 Stress Management

A common theme among the first three model dipoles (TAMU1 to TAMU3) developed at ARL is the strategy of stress management, illustrated in Fig. 10.2.

Stress management entails the integration of a high-strength support matrix within the coil, so that Lorentz forces can be intercepted and bypassed. The winding is divided into inner and outer winding blocks, in which the Rutherford cable and the wire used in each winding are graded in their composition and diameter so that the inner and outer elements operate at approximately the same fraction of the critical current.

To enforce a decoupling of forces between the inner and outer windings, a laminar spring is introduced. The laminar spring features a low compressive

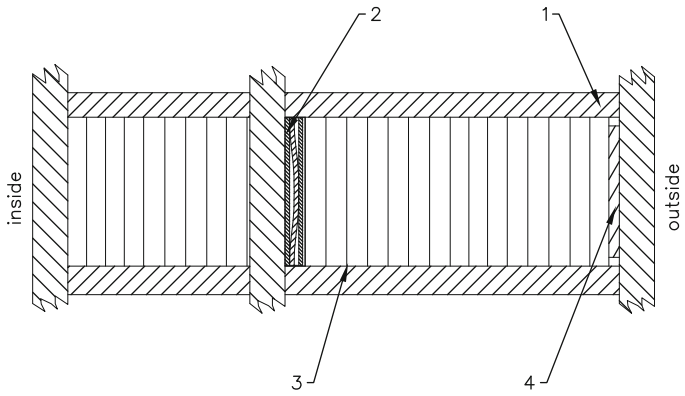

Fig. 10.2 Stress management provisions in one horizontal layer of a block-type dipole winding. *1* – Inconel piers; *2* – laminar spring; *3* – S-glass insulation and mica paper shear release; *4* – laminar strain gauge

modulus, so that very little force can be transmitted from the inner to the outer winding. Almost all the Lorentz force developed in the inner winding is intercepted on a structural beam and transferred through the flanking piers to the support matrix. The laminar spring also presents a uniform face load that maintains compression of the outer winding. The inner winding is impregnated within its compartment of the structure so that no further pre-stress is applied.

Each winding was surrounded by mica paper to provide shear release and low-friction sliding of the winding with respect to the surrounding elements of the support matrix. The mica paper does not absorb epoxy during coil impregnation, so no bonding between the coil blocks and the support matrix is established. The mica paper used, 132P from Cogebi Inc., Dover, NH, USA has a very small amount of binder (<2%), produces no ash during the Nb_3Sn heat treatment, and releases shear at the interface between piers and the coil. Shear release was verified and confirmed through considerable testing.

Because the Lorentz force acting upon the inner winding is bypassed past the outer winding, the maximum stress in any winding is limited to around 100 MPa, which is well below the limit for critical current degradation of Nb_3Sn coils.

The support matrix is made from Inconel 718. The parts are produced from material with mill finish (no surface machining), and are cut from sheet using electric discharge machining.

10.2.2 Pre-stressing the Structure

The support matrix must be loaded to compress the stress management structure so that it is preloaded and cannot move as Lorentz forces are applied within the windings. To achieve the required pre-stress the structure is preloaded with bladders. Each bladder consists of two thin stainless-steel foils, welded together around their edges to form a hermetic enclosure with a fill tube attached at one end. Each bladder is fabricated using hydraulic foil-forming and laser-weld procedures, and has been tested to five times the design pressure and twice the design expansion without failure.

In order to preload the assembled magnet, the entire assembly is heated to 80 °C, the bladders are evacuated, and molten Wood's metal (melt temperature 65 °C) is then pumped into the bladders and pressurized to 14 MPa using a hydraulic hand pump. The Wood's metal alloy Cerrolow 147 selected has near-zero aggregate temperature contraction for the cycle from 343 K to 4.2 K. The bladder's thin stainless-steel foil conforms to the finished surface of the coil assembly and flux return cavity to deliver a uniform pre-stress. By independently controlling the hydraulic pressure applied to the sets of flat and curved bladders, the preload is controlled on the entire assembly. The magnet assembly is then cooled to freeze the metal while holding the pressure.

The dipole can be disassembled by heating the magnet to 80 °C and pumping out the Wood's metal, so that the coil modules could be re-used in subsequent model

dipoles. The operation of over-compression that is used in bladder-and-key coil structures is not necessary (Caspi et al. 2001; Hafalia et al. 2003). Moreover, preload is delivered to the support structure, not to the windings themselves. The aim of applying pre-stress in this design is to make the structure stiff without applying pre-stress to the coil, so that any coil movement is blocked by the stiff structure. Relative movement between the structure and the coil is allowed, and sliding planes have been introduced to avoid any slip–slick motion and reduce training. In conventional dipole structures, preload is applied to the windings themselves, and might result in excessive strain at room temperature that could irreversibly damage Nb_3Sn filaments.

10.2.3 Flux Plate Suppression of Persistent Magnetization Fields

When a dipole is ramped from the injection field to the nominal operation field either as an accelerator or as a collider and then back to low field, eddy currents are induced at the cable, strand, and filament levels. Induced currents between strands in the cable and between filaments within a strand must pass through the copper matrix and are resistively damped. Currents induced in the individual filaments circulate entirely within the superconductor, and so can persist indefinitely (Green 1971). These persistent currents produce serious challenges for accelerator magnets. First, the pattern of induced currents produces multipole fields in the magnet aperture, which produce harmful effects upon beam dynamics. The amplitude of the multipoles induced by persistent currents depends typically on the coil geometry, the filament diameter, and the critical current density in the filaments. Second, the persistent current magnetization produces a hysteresis loop. When the magnet current is ramped down to injection, it sets the induced magnetization on the discharge trajectory. After new beam is injected and the current is ramped up as the beam is accelerated, the pattern of persistent currents re-distributes over a small range of magnetic field to that of the charging trajectory. The coil re-magnetization causes a change in the sextupole component b_3 and must be carefully compensated to avert the risk of disrupting the beam just as acceleration begins.

The block-type coil configuration uniquely makes possible a method to suppress the persistent current effect. A pair of horizontal steel flux plates are incorporated within the dipole, as shown in Fig. 10.3. We have simulated the pattern of multipoles that are induced due to persistent current effects in a block-type dipole winding, and compared the multipoles for a filament size of 50 μm and a critical current density of 2500 A/mm^2 at 4.2 K and 12 T, for the cases with and without a flux plate (Blackburn et al. 2003). The flux plate suppresses the persistent-current multipoles at 1 T injection field by a factor of 5 compared to the multipoles without a flux plate. At injection field, the flux plates are unsaturated and present a strong dipole boundary condition. Lines of force re-distribute within the flux plate to cancel multipole components.

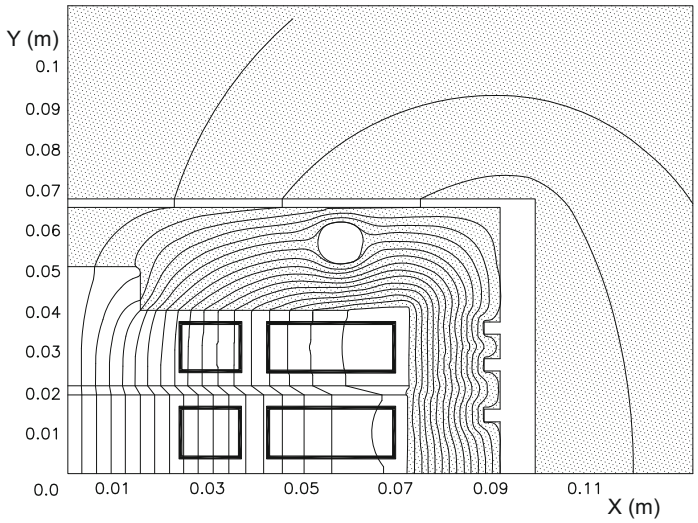

Fig. 10.3 Magnetic field distribution at injection field (1 T) for a 14 T block-type dipole. The steel flux plate (placed between the two coils) re-distributes the field lines and minimizes the sextupole component

Suppression of persistent-current magnetization is important for dipoles that will utilize Nb_3Sn, because the sub-element size in those conductors is about 50 μm, 10 times larger than the Nb-Ti filaments in the wire used for the LHC.

10.3 TAMU1: Single-Shell Nb-Ti Model Dipole

TAMU1 was designed to serve as a learning model for the construction techniques that are required for stress management: integration of the windings in the support matrix; mica paper slip surfaces; epoxy impregnation of the windings; and rectangular steel flux return. The inner and outer sub-windings are assembled within the support matrix. The windings are composed of Nb-Ti Rutherford cable and are arranged in three double-pancake winding layers, as shown in Fig. 10.4. The main parameters of TAMU1 are summarized in Table 10.2.

10.3.1 Magnet Manufacture

Each double-pancake winding was wound with an S-transition at the inner boundary. Successive double-pancake windings were connected by a splice. Before impregnation, the windings were instrumented with voltage taps, quench heaters, and spot heaters. During vacuum impregnation, the coil attained a horizontal bow of

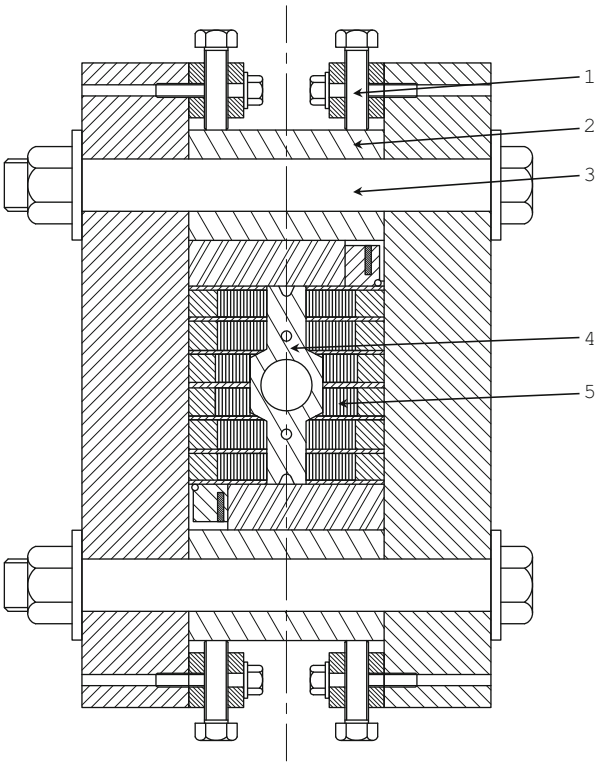

Fig. 10.4 TAMU1: first block-type prototype dipole using Nb-Ti. *1* – side compression press; *2* – compression spacer bar; *3* – main stress bolts; *4* – laminated mandrel; *5* – coil

Table 10.2 Main parameters of TAMU1

Parameter	Value
Max. field in winding (short sample) (T)	7.92
Short sample current (A)	8550
Stored energy (MJ/m)	0.10
Max. Lorentz force (MN/m)	0.47
Superconducting cable	
Number of strands	30
Strand diameter (mm)	0.808
J_c(5 T, 4.2 K) (A/mm^2)	2846
J_{Cu} at quench and short sample current (A/mm^2)	785
Cu/non-Cu ratio	1.5
Number of turns in windings	10/15/15

about 2 mm arising from a stress relieve in the fixture. This bow was corrected using smart shims to provide a uniform contact along the sides of the coil within the flux return. The coil was then installed in the structure and preloaded by using large bolts, as shown in Fig. 10.4.

Incorporation of the smart shim made it impossible to close the structure that was designed to provide stress management, so that the preload of the flux return was

delivered directly to the coil. The coil was preloaded to 500 kN, which represents about 30% of the maximum calculated Lorentz force. As the coil is excited to full field, the Lorentz force is expected to exceed the preload, and the retaining bolts should stretch elastically—the maximum bolt elongation is calculated to be around 0.20 mm. There was a concern that the resulting coil motion might produce quenches at high field; however, it did not.

Several intermittent shorts (coil to ground) were encountered during the preloading procedure, apparently arising due to a displaced insulation layer during preload. The intermittent room-temperature shorts were repaired by locating them and adding insulation in that region.

10.3.2 Testing TAMU1

The dipole was cooled to 4.5 K, and all windings were checked for turn-to-turn shorts by driving a saw tooth current waveform (20 A maximum) through the coil. The current ramp rate up was twice the current ramp rate down, so that the inductance of each winding could be checked independently at two frequencies. The voltages across coils 1 and 2 were mismatched by a ratio ~1.7, much more than the resistive mismatch ratio of 1.22 from the locations of the voltage taps, indicating that there was a turn-to-turn short, which was not found at previous testing at ambient temperature. Such a short could pose a serious hazard in a high-current quench.

A short removal scenario was attempted, in which the coil was exercised with a continuous saw tooth ramp to 300 A peak current, and the current ramp rate was increased in a succession of steps until the coil quenched from alternating current heating. The rationale was that a substantial but limited amount of energy, dumped through the short during the quench, would be sufficient to burn out the short without damaging the coil.

Each succeeding plateau corresponded to a continuous ramp to 300 A, at a series of increasing ramp rates: 50 A/s up to 600 A/s. At 600 A/s, the coil temperature reached the critical temperature $T_c = 9.3$ K, and the coil quenched. After recovery, the coil did not quench again during a repeated 600 A/s ramp sequence, but did with a 700 A/s ramp sequence. Something in the coil had changed to produce this change in behavior.

The voltages across the windings were then measured during a ramp to 300 A with 400 A/s up and 200 A/s down. All winding inductances were consistent with their calculated values L_i, indicating that the short had been successfully removed.

The quench performance of TAMU1 is shown in Fig. 10.5. TAMU1 performed close to its short sample field of 6.6 T on almost every quench showing virtually no training. There was no evidence apparent for the 20% lower current of quench #6; the location inferred from voltage taps was comparable to that of other quenches at short sample current.

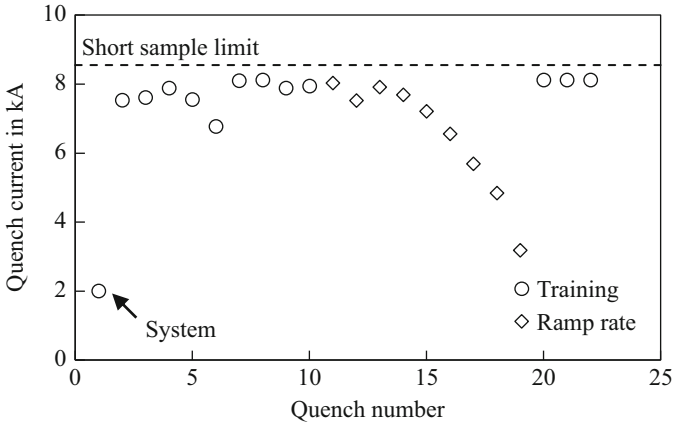

Fig. 10.5 TAMU1 quench history

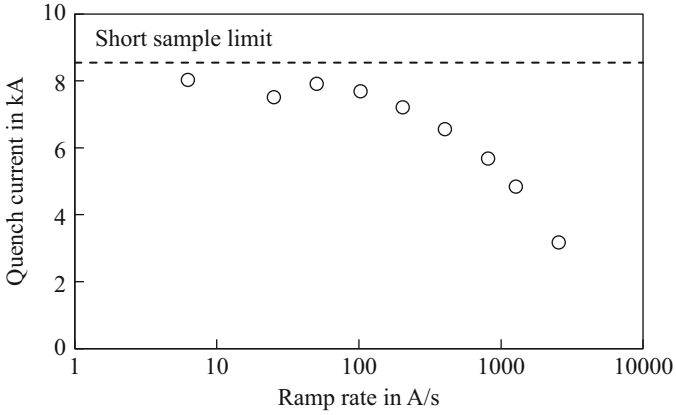

Fig. 10.6 TAMU1 ramp rate dependence

TAMU1 supported rapid ramping up to 1000 A/s (Fig. 10.6). The decrease in quench current at a ramp rate of 1000 A/s was around 50%.

10.4 TAMU2: Mirror-Geometry Nb_3Sn Dipole

TAMU2 is a two-layer Nb_3Sn dipole that contains all of the elements for stress management, and provisions for W&R heat treatment of the windings, vacuum impregnation, and preload of the reacted windings. It was designed as a mirror-magnet, so that it could be built with a single layer.

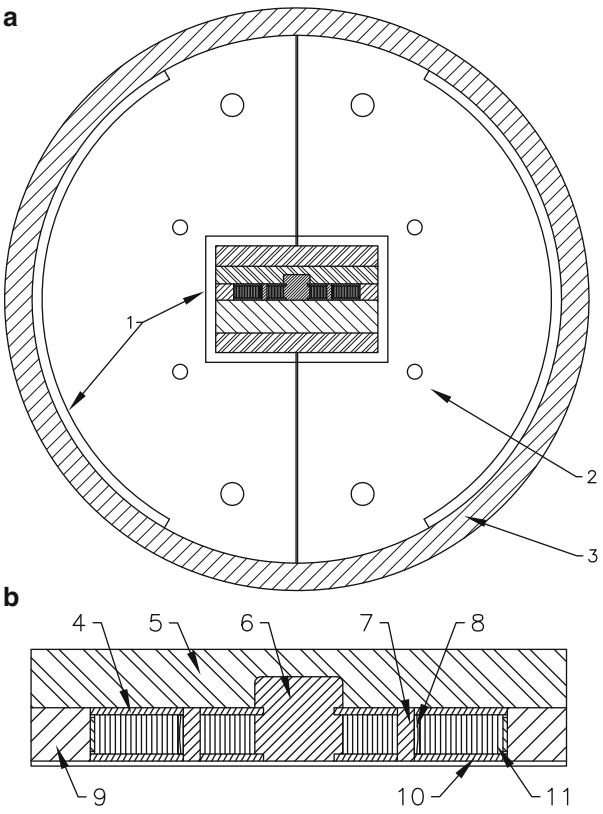

Fig. 10.7 Cross-sections of (**a**) the magnet; and (**b**) the winding module of TAMU2. *1* – spacer for inserting bladders; *2* – Fe flux return; *3* – Al stress tube; *4* – Inconel piers; *5* – Fe thick skin; *6* – Ti mandrel; *7* – Ti beam; *8* – laminar spring; *9* – Fe side bar; *10* – Fe flux plate; and *11* – laminar strain gauge

The Rutherford cable was made using International Thermonuclear Experimental Reactor (ITER)-type Nb_3Sn chrome-plated strand, which was available to ARL at no cost.

Figure 10.7 shows a cross-section of the mirror configuration. The different elements are described in detail in the following sub-sections. The main magnet parameters are summarized in Table 10.3.

10.4.1 Laminar Springs

TAMU2 was the first magnet in which laminar springs were incorporated to enforce force transfer between the inner and outer sub-windings (#8 in Fig. 10.7), as described in Sect. 10.2.1. The laminar spring is formed from annealed 0.2 mm thick Inconel X750 sheets, die-stamped to form the interior spring components, and hermetically sealed within a laser-welded Inconel shell. Hermetic sealing of the spring is vital, so that the spring enclosure does not fill with epoxy during the vacuum impregnation of the coil assembly. The springs are 13 mm wide and

Table 10.3 Main parameters of TAMU2

Parameter	Value
Max. field in coil (short sample) (T)	7.6
Short sample current (A)	10,625
Stored energy at B_{max} (MJ/m)	0.062
Max. Lorentz force at B_{max} (MN/m)	0.93
Superconducting cable	
Number of strands	30
Strand diameter (mm)	0.808
J_c(10 T, 4.5 K) (A/mm^2)	1050
J_{Cu} at quench and short sample current (A/mm^2)	1146
Cu/non-Cu ratio	0.67
Number of turns in windings	
Inner	11
Outer	16

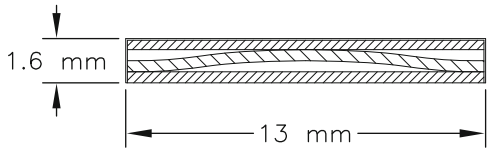

Fig. 10.8 Laminar spring cross-section

1.6 mm thick (Fig. 10.8). They have an elastic working range of 0.28 mm, the elastic range is 15% of the elongation. It is designed such that 75% of the laminar spring's deflection is used to deliver a pre-stress of about 20 MPa to the outer winding.

The laminar springs have not shown hysteresis or fatigue over 1000 cycles, which is found to be a good performance for a test magnet: The usability of this system for an accelerator-quality magnet, which is designed for tens of thousands cycles (the design number of cycles for the LHC magnets is 20,000) remains an open question.

10.4.2 Mica Paper Shear Release

Shear release was evaluated by placing the coil block in a two-axis dynamometer, applying a side load (simulating the vertical stress compressing the coil against the pier (#4 in Fig. 10.7)), and then applying a shear load to the pier until it delaminates.

The shear stress S_x required to delaminate the mica paper is a combination of the intrinsic shear S_0 within the mica and the static friction μS_y produced by the face-loading stress S_y pressing the coil block against the face of the neighboring pier: $S_x = S_0 + \mu S_y$. We impregnated a number of model coil blocks and measured S_x at a succession of levels of normal (face-loading) stress S_y. The results for the shear stress S_x are given in Fig. 10.9. Shear release occurs for $S_x < 10$ MPa so long as $S_y < 10$ MPa. The distribution of S_y has been calculated everywhere in the coil assembly, for the preloaded dipole at room temperature. Face-loading stress never exceeds 10 MPa.

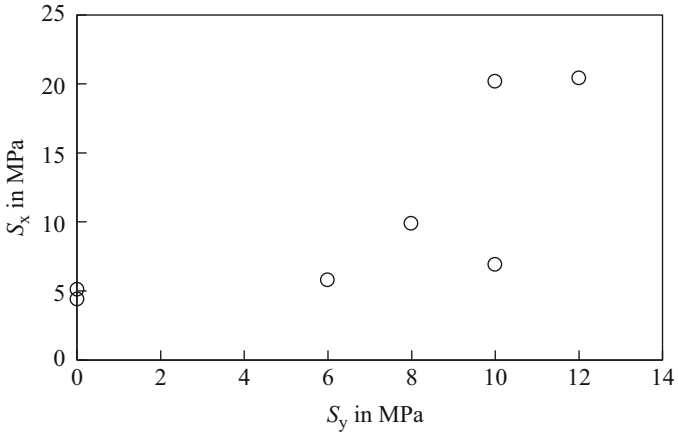

Fig. 10.9 Measured shear release stress as a function of transverse loading stress for mica paper interface in coil blocks

10.4.3 Thermal Contraction Compensation Using Ti Blocks

The axial forces on the ends of each winding are intercepted by an end support structure. This support structure is friction locked into the body of the flux return yoke. Friction locking is achieved through sufficient pre-stress in the structure. To preserve this pre-stress from ambient temperature to cool-down, small blocks of titanium are implemented which are selected such that the thermal contraction of the coil and iron in the end structure is fully compensated by the Ti blocks. The same approach was used within the coil subassemblies to maintain sufficient pre-stress in the structure.

10.4.4 Stress Transducers

Laminar pressure (stress) gauges were placed along the outer boundary of the outer winding, one along each side and one around one end (#11 in Fig. 10.7). Each transducer was prepared as a multi-layer sandwich of 316 stainless-steel foils and polyimide foils, coated with epoxy and cured under pressure to form a fully dense sandwich. Some of the stress gauges were built with five layers, some with seven layers (the capacitance response is proportional to the number of layers). The fabrication followed similar procedures developed at the European Organization for Nuclear Research (CERN), Fermi National Accelerator Laboratory (FNAL), and Lawrence Berkeley National Laboratory (LBNL), but with significant improvements that eliminated glue delamination and response creep that had plagued earlier transducers (Benson et al. 2012). Figure 10.10 shows a fabricated five-layer stress

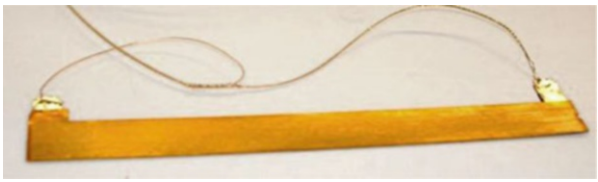

Fig. 10.10 Stress transducer

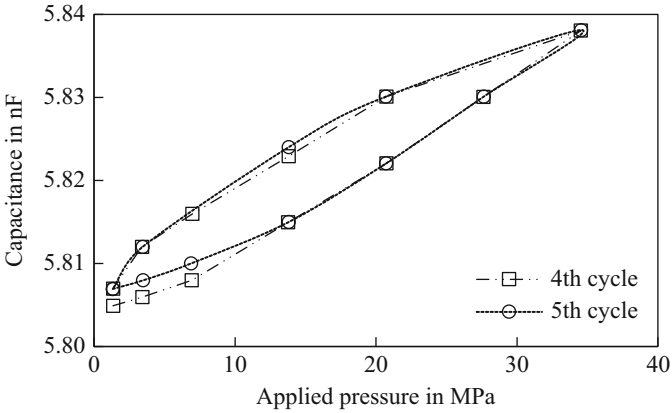

Fig. 10.11 Calibration of a stress transducer through multiple cycles

transducer. Figure 10.11 shows the calibration of a transducer over the entire range of stress from preload to full field for the fourth and fifth cycles. The calibration curve converged to a closed hysteresis curve.

10.4.5 Coil Fabrication

A double-layer coil was wound onto the laminated titanium mandrel (Fig. 10.12). The lead end of the mandrel was anchored to the support plate, and the other end of the mandrel was left unanchored, so that the mandrel could expand and contract with the winding during heat treatment. A gap of 2 mm was opened in the center of the laminated mandrel so that the net shrinkage of the winding during reaction could pull the gap closed and the winding would not be put into a strain state after heat treatment.

10.4.5.1 Heat Treatment

For the heat treatment, the coil was mounted with its side rails and end shoes in a reaction fixture that held all coil dimensions through reaction heat treatment. A removable post segment was located midway along the laminated center mandrel. It

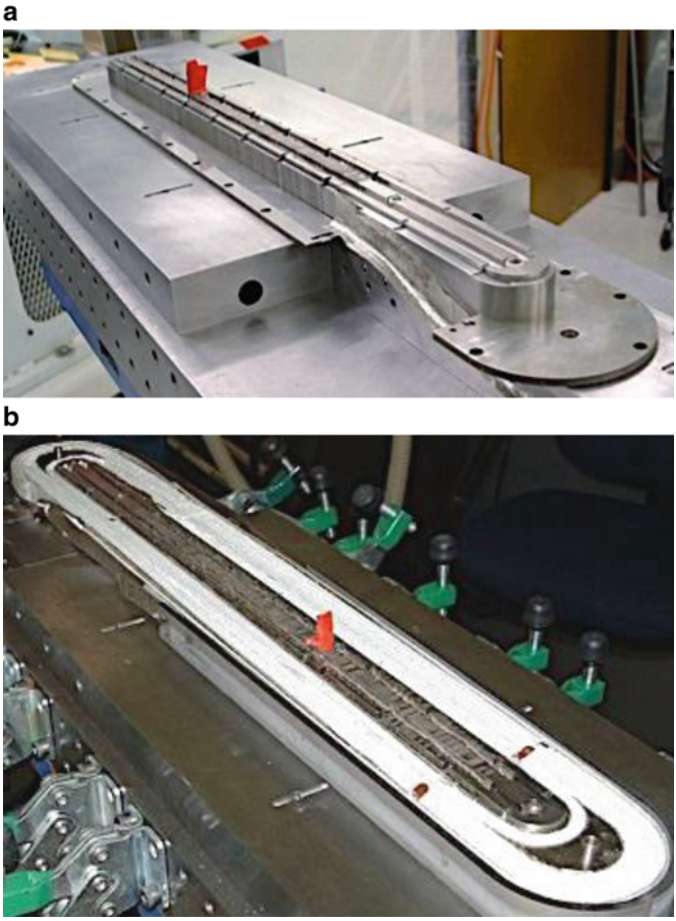

Fig. 10.12 (**a**) Winding mandrel ready for first turn; and (**b**) inner winding

was removed after coil winding before reaction, to provide room for coil axial expansion. The coil module was heat-treated: 210 °C for 100 h, 340 °C for 48 h, and 650 °C for 180 h. A purge of argon gas was maintained through the gas manifold within the reaction fixture to remove volatilized hydrocarbons from the sizing of the coil.

After heat treatment, it was observed that the pier that spans the outer layer piers was stretched. It was concluded that the deformation resulted from net elongation during heat treatment of the titanium pier (#7 in Fig. 10.7) separating the inner and outer windings and net shrinkage of the Inconel piers (#4 in Fig. 10.7), both caused by release of internal stress from the rolling of the original sheet materials. The coil was not visibly damaged and the assembly of the module and of the dipole was continued. In subsequent tests, rolling stresses were released by performing a stress relief heat treatment before machining.

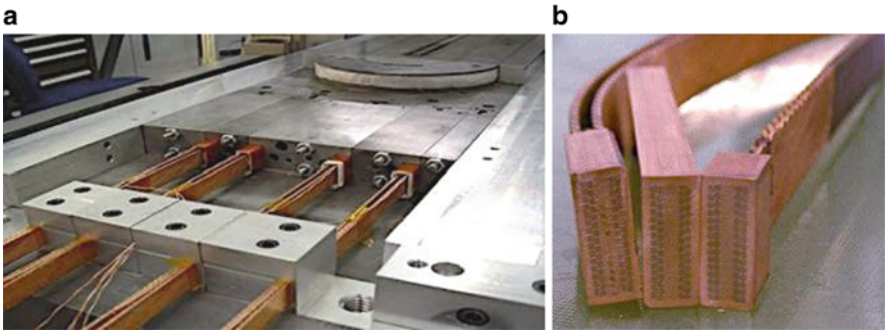

Fig. 10.13 (**a**) Splicing of Nb-Ti lead cables onto Nb_3Sn windings; (**b**) cross-sections of test splices

10.4.5.2 Nb_3Sn to Nb-Ti Cable Splicing

Each Nb_3Sn lead was spliced to a pair of flexible Nb-Ti cables. During heat treatment, each lead segment of Nb_3Sn cable is supported within a removable channel, so that it cannot deform. After heat treatment, the segments of the channel are removed and a pair of Nb-Ti cables is assembled to sandwich the Nb_3Sn lead. The sandwich contains flat strips of fluxed low-melt SnAg solder between successive layers. The support channel is then re-assembled and heater cartridges are energized to heat the joint to the flow temperature of the solder. The process was developed to produce a fully soldered joint from each face of the Nb_3Sn lead to an Nb-Ti cable. Measured splice resistance was 0.28 nΩ. The splicing and the joints are shown in Fig. 10.13.

10.4.6 Structure Assembly

The flux return yoke is divided into two halves in the vertical mid-plane surrounded by a super-alloy aluminum stress shell. The coil assembly surrounded by flat bladders is inserted into the rectangular cavity of the flux return. The flux return itself is preloaded by the pair of curved bladders that are inserted into the aluminum stress shell.

To achieve the required pre-stress, a set of four flat bladders supports the coil module in the box space within the two halves of the steel flux return (#1 in Fig. 10.7). Another pair of curved bladders are located in a space between the outside surface of the flux return steel and the super-alloy aluminum stress shell. This shell provides the overall containment of all forces and additional pre-stress during cool-down thanks to its larger thermal contraction factor.

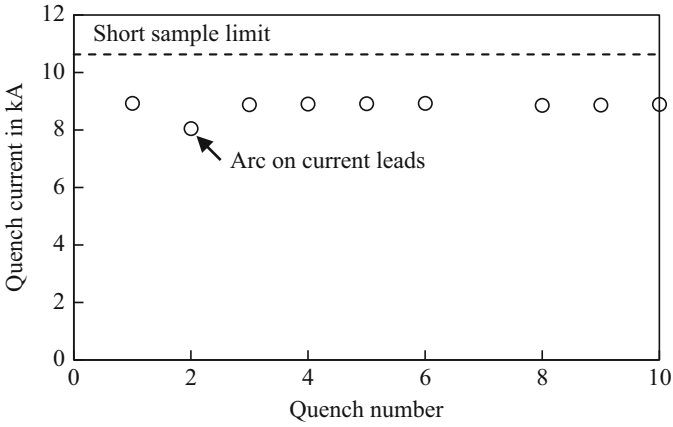

Fig. 10.14 Quench history of TAMU2 (data for quench #7 was lost due to a defect in the data acquisition)

10.4.7 Testing of TAMU2

The magnet was tested in boiling LHe at 4.4 K at LBNL. The chronological quench history of TAMU2 is given in Fig. 10.14. The ramp rate for training quenches was 10 A/s. The cable and strand data available at the time of construction indicated that the short sample current for TAMU2 is 8914 A. Short samples of the same wire were wound on an ITER barrel, heat-treated by the same schedule, and tested for short sample current $I_c(B)$. The dipole quenches in Fig. 10.14 correspond to 93.4% of witness strand short sample currents. There was no training: within the small spread in quench current values observed: the magnet went to the same value every quench. The best recent performance for cable made from ITER strand would have resulted in a short sample current of 9633 A in the windings of TAMU2.

Some excitement came with quench #2. As current was ramping up towards the previous quench value, a peculiar clanking sound was heard from the region of the Cu bus bar channels that carry current to the test cryostat. Just as we were endeavoring to find its origin, a flash of light and an explosive bang came from the same location. A large bolt had been left on top of one of the Cu bus bars during preparations for the test. Although made from stainless steel the bolt had no small permeability. When the bus current reached ~8 kA, the bolt magnetically levitated, and by the second cycle happened to shift in position to make a short circuit between the side-by-side bus bar leads. After repair of the test station the magnet training was continued, and magnet training ramp rate studies were continued to be performed. For the ramp rate studies, the coil current was ramped successively faster and the quench current was measured. The ramp rate dependence is plotted in Fig. 10.15. It was anticipated that coupling currents would be suppressed by the orientation of the cable parallel to the magnetic field in the windings. As previously mentioned, the conductor was chrome-plated, which increased the contact resistance between strands and therefore aided in the suppression of coupling currents. Nevertheless, the extreme robustness of TAMU2 for fast ramp rates was

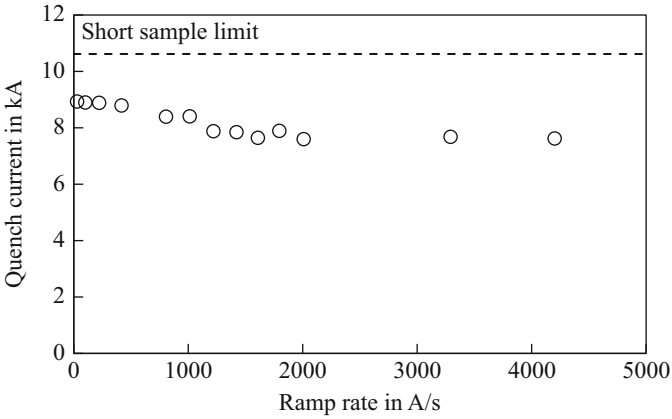

Fig. 10.15 Ramp rate studies of TAMU2

surprising. The only limitation that was encountered was the power supply's inability to regulate with the low inductance of TAMU2 at very high ramp rates (>2000 A/s). For these points, the stated ramp rate value was estimated from the current read-back data. The ramp rate data indicates that an Nb_3Sn block-coil dipole could be suitable for cycling at a few T/s in the 6 T field range, a topic of interest for future fast-cycling accelerator projects.

10.5 TAMU3: 13 T Racetrack Dipole

TAMU3 is an Nb_3Sn block-type dipole built to embody all the above provisions for stress management. Its flat racetrack coils were built as two identical modules, each containing an inner and outer winding, as shown in Fig. 10.16. The inner and outer windings were graded—the strand size in each was chosen so that the inner and outer windings would operate at the same fraction of short sample limit. The strands intended for both windings were 54/61-filament restacked rod process (RRP) Nb_3Sn produced by Oxford Instruments Technology, USA. Table 10.4 summarizes the main parameters of TAMU3.

10.5.1 Fine-Filament S-Glass Insulation

An improved S2-glass fabric insulation was developed for use in the Nb_3Sn windings of TAMU3. Following some lead development at the Commissariat à l'énergie atomique (CEA) in Saclay, France (Canfer et al. 2008), the company AGY, Aiken, SC (www.agy.com), produced a fine-filament S2-glass yarn containing 204 filaments of 5.5 μm diameter with a linear mass density of 11 tex (g/km). The yarn was treated

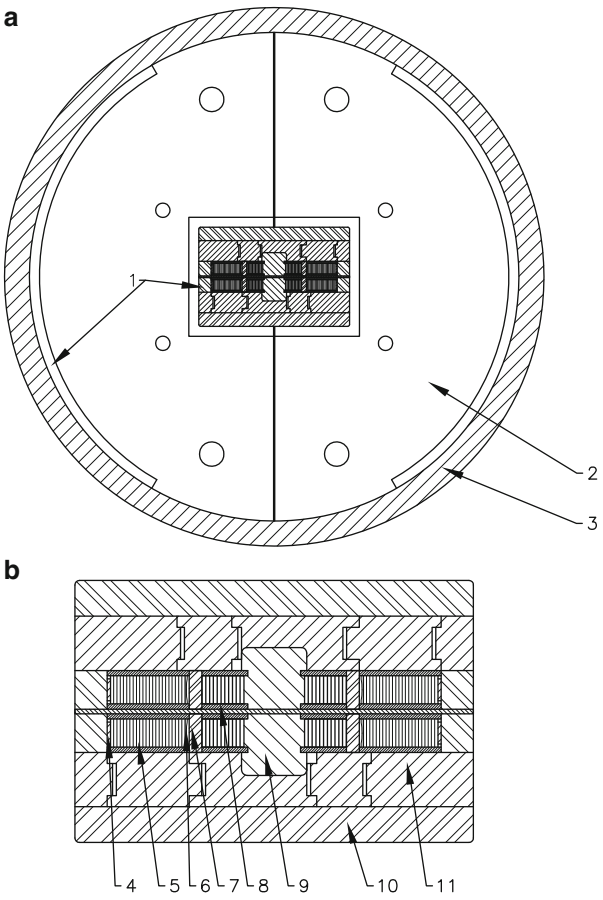

Fig. 10.16 Stress management elements in TAMU3. (**a**) The magnet: *1* – bladders; *2* – Fe flux return; *3* – Al stress tube; (**b**) the coil: *4* – stress transducers; *5* – Inconel piers; *6* – laminar spring; *7* – Ti beams; *8* – Mica shear release; *9* – Ti central mandrel; *10* – Fe filler; *11* – Fe side bar

with a silane-based sizing. Silane sizing is stable under the 650 °C heat treatment required for Nb_3Sn. Silane provides the benefit of promoting enhanced surface adhesion between epoxy and the S2-glass.

To braid this yarn onto the Rutherford cable the company A&P Technology, Cincinnati, OH developed in collaboration with ARL a forming guide and stabilizing technique to secure the Rutherford cable during processing (Blackburn et al. 2008b). A uniform, tight-weave fabric with a compressed thickness of 55 μm/side was produced. Figure 10.17a shows the fabric direct-woven onto the cable for TAMU3; Fig. 10.17b shows a micrograph of the yarn in the fabric.

10.5.2 Mechanical and Electrical Characterization

To perform mechanical and electrical testing, 10-stack assemblies of cable segments were stacked, compressed, and vacuum-impregnated. The 10-stack samples were

Table 10.4 Main parameters of TAMU3

Parameter	Value
Max. field in coil (short sample) (T)	14.1
Short sample current (A)	13,750
Stored energy at B_{max} (MJ/m)	0.425
Max. Lorentz force at B_{max} (MN/m)	1.76
Superconducting cable inner layer	
Number of strands	30
Strand diameter (mm)	0.808
J_c(10 T, 4.5 K) (A/mm^2)	2750
J_{Cu} at quench and short sample current (A/mm^2)	2047
Cu/non-Cu ratio	0.67
Superconducting cable outer layer	
Number of strands	34
Strand diameter (mm)	0.70
J_c(10 T, 4.5 K) (A/mm^2)	2750
J_{Cu} at quench and short sample current (A/mm^2)	2097
Cu/non-Cu ratio	1.0
Number of turns in windings	
Inner	11
Outer	23

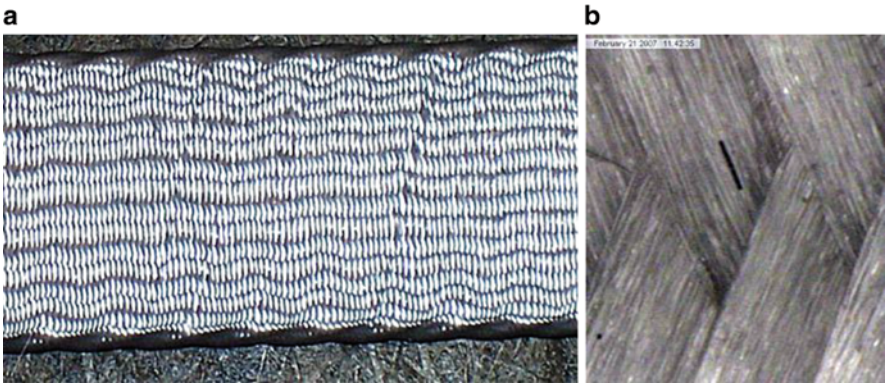

Fig. 10.17 (**a**) Thin-filament silane-sized S2-glass fabric direct-wound on Nb_3Sn Rutherford cable for TAMU3); (**b**) micrograph of yarn in the fabric

tested for mechanical strength against delamination and for electrical strength of turn-to-turn insulation. The interfaces were delaminated at a pressure of 33 MPa, corresponding to a shear stress of about 5 MPa. Similar tests were made using segments of windings from the TAMU2 dipole, which were prepared using conventional S2-glass insulation technology. The shear strength of the new fabric was about 20% higher than that of the segments from TAMU2. The improvement was attributed to the silane, retaining its adhesion-promoting benefits even after 650 °C heat treatment.

The 10-stack samples were instrumented to measure turn-to-turn dielectric strength within an impregnated coil. First, voltage was applied between the two outermost turns of the 10-stack. Up to an applied voltage of 3 kV, corresponding to a local electric field of about 3 MV/m, the resistance was greater than 130 GΩ. Second, voltage was applied between adjacent turns throughout the stack. The resistance was larger than 130 GΩ up to >300 V/turn. These results are acceptable for this magnet. The volume fraction of insulation within the coil is about 7%, compared with 12–20% for conventional insulation. The thinner insulating layer should improve heat transfer for quench protection of high-stored-energy magnets.

10.5.3 Heat Treatment

A heat treatment of 210 °C for 48 h, 340 °C for 48 h, and 670 °C for 70 h was employed to maximize the critical current density in the windings. Tin leakage was observed on the exposed face of the inner winding of the first module, at locations between the third turn and the ninth turn of the inner conductor. One tin leak is shown in Fig. 10.18. It was 1.5 cm long and occurred 15 cm away from the inner lead end.

Tin leakage was not expected, so it was puzzling that multiple tin leaks had occurred. Extracted samples of wire from a reacted witness sample were sent to the National High Magnetic Field Laboratory (NHMFL) for measuring the critical current I_c. The results showed a resistive onset at about 400 A, at around half the critical current expected in the RRP wire. We investigated the source of the wire, and found that a spool of long-obsolete modified jellyroll (MJR) wire had been shipped to us by mistake for use in the inner winding. This mistake resulted in a

Fig. 10.18 Tin leakage at turn 3 of the inner winding of one module

compounding of errors, with the effect that the short sample current and field was almost halved; from an expected 13.75 kA to 7.8 kA.

This dreadful pair of mistakes were discovered at a time when the modules had been completed, and the funding and schedule could not accommodate re-fabricating both modules. We had no choice but to complete the magnet assembly and test it to its severely compromised short sample limit.

10.5.4 Testing TAMU3

TAMU3 was tested at the Brookhaven National Laboratory (BNL) magnet test facility in a liquid He bath at 4.4 K. The first quench occurred at 5695 A (73% of the expected short sample limit on load line). On subsequent quenches a modest degree of training was observed—quench current improved to a plateau of around 6600 A (85% on load line), corresponding to 7.57 T in the center bore of the dipole.

The locations of the quenches were estimated from the timing of quench arrival at each of the voltage taps on the inner winding. The quench initiated at the location where the outer lead of the inner winding is hard-way bent and then guided along a lead channel in the strong back structure of each module. That location is indicated by the blue arrow in Fig. 10.19.

We concluded that the conductor was damaged in that location in one of the modules. Indeed, the MJR conductor was severely embrittled in the high-temperature heat treatment that was used for the TAMU3 windings, so the extra

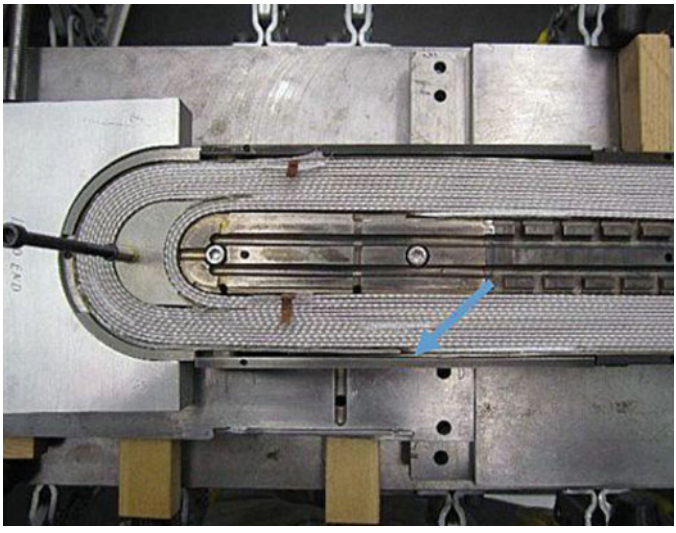

Fig. 10.19 TAMU3 winding showing the location where quenches originated

stress of the hard bend for the lead may have produced a weak point location for damage.

We learned a bitter lesson from the experience of TAMU3: it is vital to perform short sample measurements on samples of all wire that will be used in a dipole, in order to avoid mistakes of the kind that cost the performance of this dipole. Another important lesson was that enough space for coil expansion during reaction needs to be provided to avoid high stresses of the coil during the heat treatment in the reaction mold.

10.6 Conclusion

A succession of dipoles has been built using block-type coil geometry and stress management elements. TAMU1 first introduced stress management. TAMU2 introduced stress management in an Nb_3Sn dipole for the first time, and achieved remarkable ramp rate performance. TAMU3 introduced a fine-filament S2-glass insulation that enhances mechanical and electrical properties of an impregnated winding. Unfortunately, a mistake in the conductor used in one winding severely compromised the magnet's performance.

Block-type geometry naturally accommodates stress management within windings in the body of the dipole, and provides just as efficient use of superconductor as do other coil geometries. It is the only coil geometry that can accommodate a flux plate to suppress persistent-current multipoles from magnetization of filaments within the cables.

The difference in amount of superconductor for the block-type and shell-type (also known as cos-theta) coil design under the same assumptions is small. The choice of cable and coil geometry for any application should be based upon the field homogeneity, cryogenic stability, robustness against strain degradation, support of flared ends, manufacturability, compatibility with hybrid-coil strategies, and overall collider cost per TeV.

Recently, ARL has developed a coil-forming technology that enables rapid, precise forming of compact flared ends for windings based on CIC conductor. ARL believes that this conductor type offers a promising basis for high-field collider dipole development, in that it addresses each of the challenges that pace such development:

- Stress is managed at the cable level and is intercepted by sheath tubes and beams;
- Beams precisely position each cable turn;
- A simple winding procedure provides stability against de-registration when forming flared ends;
- Strands are bathed in LHe within the cable, the mechanical stability is provided by the metallic support structure, and no impregnation around the strand is required, which enhances stability against micro quenches;

- CIC provides the possibility of argon buffer gas flow during Nb_3Sn heat treatment;
- CIC can be made with sheath and center tubes from Al-bronze to suppress cation migration during Bi-2212 heat treatment;
- CIC provides the possibility of O_2 gas purging within the sheath tube at high pressure to support Bi-2212 over-pressure processing without exposure to the overall furnace and dipole components.

In a recent paper (McIntyre et al. 2018) ARL presented two designs for CIC-based hybrid-coil dipoles suitable for operation at 16 T. The quantity of superconducting wire in each is similar than that in high-field designs currently being developed using Rutherford cable. The work on this concept continues at ARL.

References

Assadi S, Chavez D, Gerity J et al (2015) Magnet design and synchrotron damping considerations for a 100 TeV hadron collider. In: Henderson S et al (eds) Proceedings of the international particle accelerator conference IPAC2015, Richmond, 5 May 2015, pp 4034–4037

Assadi S, Breitschopf J, Chavez D et al (2017) Cable-in-conduit dipoles to enable a future hadron collider. IEEE Trans Appl Supercond 27(4):1–5. https://doi.org/10.1109/tasc.2017.2656157

Battle C, Blackburn R, Diaczenko N et al (2001) Testing of TAMU1: a single-aperture block-coil dipole. In: Lucas P, Webber S (eds) Proceedings of the 2001 particle accelerator conference (Cat. No.01CH37268), Chicago, 18–22 June 2001, vol 5, pp 3642–3644

Benson CP, Holik EF III, Jaisle A et al (2012) Improved capacitive stress transducers for high field superconducting magnets. Advances in cryogenic engineering: transactions of the cryogenic engineering conference—CEC, vol 57. AIP Conf Proc 1434(1):1337–1344. https://doi.org/10.1063/1.4707059

Blackburn R, Elliott T, Henchel W et al (2003) Construction of block-coil high-field model dipoles for future hadron colliders. IEEE Trans Appl Supercond 13(2):1355–1357. https://doi.org/10.1109/tasc.2003.812667

Blackburn R, Diaczenko N, Elliott T et al (2008a) Fabrication of TAMU3, a wind/react stress-managed 14 T Nb_3Sn block coil dipole. J Phys Conf Ser 97(012128). https://doi.org/10.1088/1742-6596/97/1/012128

Blackburn R, Fecko D, Jaisle A et al (2008b) Improved S-2 glass fabric insulation for Nb_3Sn Rutherford cable. IEEE Trans Appl Supercond 18(2):1391–1393. https://doi.org/10.1109/tasc.2008.920762

Canfer S, Ellwood G, Baynham DE et al (2008) Insulation development for the next European dipole. IEEE Trans Appl Supercond 18(2):1387–1390. https://doi.org/10.1109/tasc.2008.921862

Caspi S, Gourlay S, Hafalia R et al (2001) The use of pressurized bladders for stress control of superconducting magnets. IEEE Trans Appl Supercond 11(1):2272–2275. https://doi.org/10.1109/77.920313

Diacaenko N, Elliott T, Jaisle A et al (1997) Stress management in high-field dipoles. In: Comyn M et al (eds) Proceedings of the 1997 particle accelerator conference, Vancouver, 12–16 May 1997. IEEE, Piscataway, pp 3443–3445

Elliott T, Garrison R, Holik T et al (2016) Testing of TAMU3: an Nb_3Sn block-coil dipole with stress management. U.S. Department of Energy, Office of Scientific and Technical Information report, Oak Ridge, TN, DOE-TAMU-11685-5

Green MA (1971) Residual fields in superconducting dipole and quadrupole magnets. IEEE Trans Nucl Sci 18(3):664–668. https://doi.org/10.1109/tns.1971.4326146

Hafalia R, Caspi S, Chiesa L et al (2003) An approach for faster high field magnet technology development. IEEE Trans Appl Supercond 13(2):1258–1261. https://doi.org/10.1109/tasc.2003.812632

Holik EF, McInturff AD, Benson CP et al (2011) Current progress of TAMU3: a block-coil stress-managed high field (>12 T) Nb_3Sn dipole. In: Satogata T, Brown K (eds) Proceedings of the particle accelerator conference, New York, 26 Mar–1 Apr 2011. IEEE, Piscataway, pp 1163–1165

Holik EF, Garrison R, Diaczenko N et al (2014) Construction challenges and solutions in TAMU3, a 14 T stress-managed Nb_3Sn dipole. In: Adv Cryo Eng: AIP conference proceedings vol 1573, pp 1535–1542

Kashikhin VV, Zlobin AV (2001) Correction of the persistent current effect in Nb_3Sn dipole magnets. IEEE Trans Appl Supercond 11(1):2058–2061. https://doi.org/10.1109/77.920260

McInturff A, Bish P, Blackburn R et al (2007) Test results of an Nb_3Sn wind/react "stress-managed" block dipole. IEEE Trans Appl Supercond 17(2):1157–1160. https://doi.org/10.1109/tasc.2007.898437

McIntyre P, Breitschopf J, Chavez D et al (2018) Block-coil high-field dipoles using superconducting cable-in-conduit. IEEE Trans Appl Supercond 28(3):1–7. https://doi.org/10.1109/tasc.2018.2797915

Noyes P, Blackburn R, Diaczenko N et al (2006) Construction of a mirror-configuration stress-managed Nb_3Sn block-coil dipole. IEEE Trans Appl Supercond 16(2):391–394. https://doi.org/10.1109/tasc.2006.871326